Supporting Information

Spin-Correlated Radical Pairs as Quantum Sensors of Bidirectional ET Mechanisms in Photosystem I

Oleg G. Poluektov*, Jens Niklas, Lisa M. Utschig*

[†]Chemical Sciences and Engineering Division, Argonne National Laboratory, 9700 S. Cass Ave., Lemont, IL 60439, USA,

**To whom correspondence should be addressed. E-mail: Oleg@anl.gov; Utschig@anl.gov*

Materials and Methods

Sample preparation. PSI reaction centers were extracted from 99% deuterated cyanobacterium *Synechococcus leopoliensis*[1] as described previously.[2] Purified PSI was prepared in 50 mM MES, pH 6.5, 20% glycerol, 0.03% β-DM (*n*-dodecyl β-D-maltopyranoside, Anatrace), 30 mM sodium ascorbate. The [4Fe-4S] clusters were removed by established preparations. PSI (0.2 mg Chl/ml) was incubated in a buffer containing 6.8 M urea, 62 mM Tris, 76 mM glycine-NaOH, pH 10, for 1 h, as previously described to remove F_A/F_B.[3] The PSI sample was then dialyzed overnight against 50 mM Tris-HCl pH 8.3. To remove F_X, the sample was further treated with 3 M urea, 5 mM K_3FeCN_6, 50 mM Tris-HCl, pH 8.0, for 4.5 h.[4] The PSI sample was dialyzed overnight against 50 mM Tris-HCl, pH 8.3, and 5 mM 4,5-dihydroxy-1,3-benzene-disulfonic acid (disodium salt), and then again overnight against 2 changes of 50 mM Tris-HCl, pH 8.0, 0.03% β-DM. The sample, analyzed by ICP-AES, showed a ratio of ~1 Fe/PSI monomer after urea treatment, confirming removal of the three [4Fe-4S] clusters. For EPR, the Fe-removed PSI sample was concentrated to 150 μM PSI monomer with final conditions of 50 mM Tris-Cl, pH 8.3, 20% glycerol, 0.03% β-DM, and 10 mM sodium ascorbate. Chemically reduced Fe-removed PSI samples were prepared in 50 mM glycine-KOH pH 9.87, 20 % glycerol, 0.03% β-DM and 40 mM sodium hydrosulfite. Chemically reduction in combination with photochemical reduction was accomplished by treating PSI samples with either 0.1 M sodium ascorbate in 50 mM MES-NaOH buffer, pH 6, or 0.2 M sodium hydrosulfite in 2 M glycine-KOH buffer, pH 10. Final reductant concentrations were ~10 mM for sodium ascorbate and ~40 mM for sodium hydrosulfite. All samples were dark-adapted for ~15 minutes at room temperature. This procedure leads to the reduction of F_A and F_B iron-sulfur complexes in the sodium hydrosulfite containing samples. The reduction of F_X and A_{1A} was achieved by illumination of these samples at 205-245 K followed by rapid freezing to 100 K.

The samples were loaded into quartz tubes (inner diameter 0.5 mm / outer diameter 0.6 mm), dark-adapted, and placed in the microwave cavity. The cavity was held in an Oxford flow cryostat, and temperature was controlled by the Oxford temperature control system. Sodium ascorbate containing samples were cooled down to 100 K in the dark. Sodium hydrosulfite containing samples were cooled down to 205 – 245 K in the dark, followed by illumination for various time durations with Laser light.

EPR spectroscopy. EPR measurements were performed on a pulsed/continuous wave high-frequency D-band (130GHz/4.6T) EPR spectrometer[5-6] with single mode cylindrical cavity TE_{011}. Pulsed TR-EPR spectra of the spin-correlated radical pairs (SCRP) were recorded by monitoring the electron spin echo (ESE) intensity from a two microwave pulse sequence, which followed a

short (<10 ns) Laser pulse at a fixed Delay After Flash (DAF) time, as a function of magnetic field. Decay kinetics of the transient radical species were measured by recording the intensity of the ESE signal at a particular magnetic field value as a function of the DAF time. The duration of the $\pi/2$ microwave pulse was 40-60 ns and typical separation times between microwave pulses were 200-300 ns. Light excitation of the sample was achieved with an optical parametric oscillator (OPO; BasiScan from GWU) pumped by a Nd:YAG Laser (Quanta-Ray INDI, Spectra Physics), the output of which was coupled to an optical fiber. The optical fiber allows delivery of up to 2 mJ per pulse to the sample. Excitation wavelength was 550 nm.

The theoretical SCRP spectra were simulated using an approach described previously.[7-8]

Spin Correlated Radical pairs $P^+A_{1A}^-$ and $P^+A_{1B}^-$ in Photosystem I

The EPR spectra of spin-correlated radical pairs (SCRPs) in a defined orientation within a protein like PSI are in several aspects different from the EPR spectra of isolated, non-interacting radicals. For a detailed introduction to the theory of SCRPs, the reader is referred to the literature.[8-18] Here, only a qualitative description is provided for the specific case of a weakly coupled SCRP created by fast ET as is the case for PSI.

For the simpler case of two interacting radicals in thermal equilibrium, four distinct energy levels exist with the lower levels being preferentially populated (Boltzmann distribution; Figure S1 left). The radical with smaller g-factor shows at the same magnetic field a smaller energy difference between the electron spin levels and thus becomes resonant at higher magnetic fields. The magnetic interactions between the distant cofactor radicals P^+ and A_1^- in PSI (≈25 Å) are small in comparison to the differences in resonance frequencies of the non-interacting radicals at high fields/high frequencies like D-band ($|J|$, $|D| << |Q|$).[19-20] It is important to note, that this weak coupling limit is typically not a good approximation at standard EPR field/frequencies like X-band (9.5 GHz/0.34 T), where the electron Zeeman interaction is about an order of magnitude smaller. The exchange interaction J is so small for the RP P^+ A_1^- in PSI that it can be neglected for any qualitative discussion (see Table S1). All nuclear hyperfine interactions are substantially smaller than the dipolar interaction D and the g-tensor anisotropy at D-band and thus don't have to be explicitly considered but only contribute to the line width (see Table S1). The dipolar interaction between the two spins leads to a doublet of lines for each radical (instead of a single line), due to the dependence on the spin state of the other electron. The complete powder spectrum is obtained by integration over all possible orientations of PSI in the magnetic field with its cofactors in a fixed geometry with respect to each other. Note, that EPR spectra recorded in pulsed mode

are exhibiting absorptive-type line shapes and not derivative-type line shapes as typically seen in continuous wave EPR. In a SCRP which is rapidly generated by ET from a photoexcited singlet state, only the states with partial singlet character (|2>, |3>) are populated, while levels |1> and |4> are empty (Figure S1 c). That results in both absorptive and emissive lines (antiphase doublets), which have the appearance of a derivative lineshape if the line width is larger than the splitting between the doublet. A change in temperature thus has no direct influence on the SCRP spectra, while the spectra of a stable, thermalized radical pair will increase in intensity with decreasing temperature in a way similar to an isolated radical.

The lineshapes of the two SCRP spectra assigned to $P^+A_{1A}^-$ and $P^+A_{1B}^-$ (Figures S1f, and Figure 3 in the manuscript) are clearly different, particularly in the high field parts of the spectra. As mentioned above, according to the model for SCRP EPR spectra in the limit of weak dipolar and exchange interactions, the lineshape of the SCRP spectrum can be described as the sum of two contributions from the two constituents of the secondary radical pair, P^+ and A_1^- in the case of PSI. The lineshapes of these contributions depend primarily on the direction of the interspin vector connecting the radicals in the g-tensor axes of the corresponding radical (see Figure S1d). The A_1^- low field spectral contributions from $P^+A_{1A}^-$ and $P^+A_{1B}^-$ in Figure 3 of the manuscript have similar lineshapes. This is in agreement with the PSI structure, where the orientations of quinones are highly symmetric relative to the primary donor, so that the angles of the vectors directed from each quinone to P^+ are similar in the g-tensor principal axes of the respective quinone (Figure S1d). In the case of P^+, the situation is different. The distinctions between the high-field region of the spectra (where the lineshape is determined by the P^+ part of the SCRP), indicates that the directions of the P^+ - A_{1A}^- and P^+ - A_{1B}^- interspin vectors are not symmetric in the g-tensor principal axes of P^+ (Figure S1d).

The simulated spectra are in good agreement with the experimental spectra (Figure 3 of the manuscript). Simulations were performed assuming the same g-tensor axes for the two quinones. The small shift in g_X of the two quinones A_{1A}^- and A_{1B}^- in the respective radical pairs as well as the difference in the line widths (see Table S1) was taken into account.

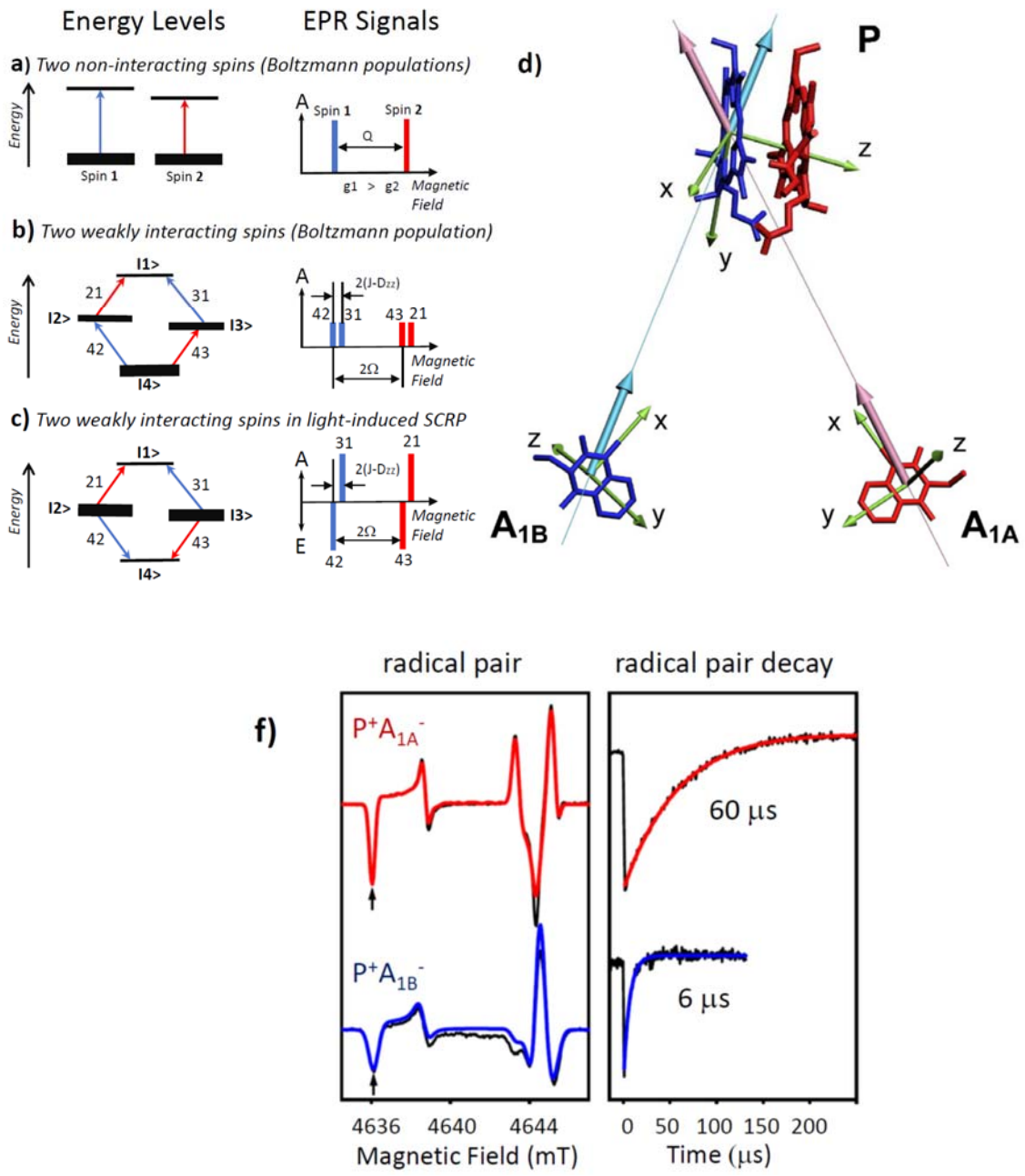

Figure S1. Left. Energy levels and EPR (stick) spectra in a weakly coupled (|J|, |D|<<|Q|) radical pair (RP). The thickness of the energy levels indicated the population. The position of the EPR line above or below the field axis indicates absorption (A) or emission (E), respectively. **a.** Two isolated (non-interacting) spins with different g-values (g_1>g_2). **b.** Two weakly interacting spins with different g-values (g_1>g_2) in thermal equilibrium (Boltzmann distribution). The interaction between the two spin leads to a doublet of lines for each radical with a splitting of 2(J-D_{zz})). The difference between the transitions 42 and 43 or 31 and 21 is 2Ω, with $\Omega^2 = (J+½D_{zz})^2 + Q^2$. Note, that dipolar interaction and difference in resonance frequencies of the

isolated radicals (Q) depends on the orientation of the protein with respect to the magnetic field. **c.** Spin-correlated radical pair (SCRP) with population only of states with partial singlet character (|2>, |3>), leading to absorptive and emissive lines (antiphase doublets). In case of negligible J and D<0, the polarization pattern E/A/E/A is observed for orientations with <54.7°. Line positions and splittings are identical to thermalized RP shown in **c.**

Right (d). Relative orientation of the primary electron donor P and electron acceptors A_{1A} and A_{1B}, taken from the X-ray crystal structure.[21] Cofactors in the A and B chains are marked by red and blue, respectively. Note, that the color coding here is not related to the color coding used in **a,b,c.** The localization of the primary donor spin density was chosen on the B half of the P dimer.[22-23] This assumption is not relevant for the data analysis and does not affect the conclusions. Green arrows show the directions of the main axes of the radical g-tensors. Interspin dipolar axis in the A-branch is shown by pink vector, and in the B-branch by light-blue vector. Note that while the orientations of these vectors are similar in the g-tensors axes of A_{1A}^- and A_{1B}^-, they are very different in the g-tensor axes of P^+. As a result, the lineshapes of the low-field portions of the SCRP spectra $P^+A_{1A}^-$ and $P^+A_{1B}^-$ (Figure 3 of the manuscript) are very similar, but the high-field parts are substantially different.

Bottom (f). High frequency (130 GHz) TR-EPR spectra and corresponding decay kinetics of PSI complexes from perdeuterated cyanobacterium *Synechococcus lividus* at 100 K. Black lines – experimental data; red lines – simulation of SCRP in the A branch, $P^+A_{1A}^-$; blue lines – simulation of SCRP in the B-branch, $P^+A_{1B}^-$. Decay kinetics are recorded at quinones' g_x field positions, marked with arrows.[19]

Table S1. Magnetic resonance and structure parameters used for simulations of the EPR spectra.[19]

	g-tensor principal values, $(g_i-2)*10^4$, where i = X, Y, Z			line width, mT[a]		
	X	Y	Z	X	Y	Z
P^+	32.2	27.7	24.6	0.34 (0.45)[b]	0.22 (0.42)[b]	0.29 (0.52)[b]
A_{1A}^-	63.6	52.0	23.1	0.25	0.25	0.25
A_{1B}^-	62.9	52.0	23.1	0.47	0.44	0.44
A_0^-	41.3	31.5	22.1	0.60	0.46	1.20

	magnetic interactions		dipolar axis directions in			
			P^+ g-tensor axes		A_1^- g-tensor axes	
	D^c, mT	J^c, μT	φ^d	θ^d	φ^d	θ^d
$P^+A_{1A}^-$	-0.17	5	63°	39°	0°	79°
$P^+ A_{1B}^-$	-0.17	1	52°	90°	1°	88°

[a] Line broadening, e.g. due to unresolved hyperfine interactions (hfi), was simulated by a Gaussian lineshape with widths shown in the table.

[b] Values in parenthesis were used for simulation of $P^+A_{1B}^-$.

[c] D and J – dipolar and exchange interactions, respectively.

[d] φ and θ – azimuthal and tangential angles, respectively.

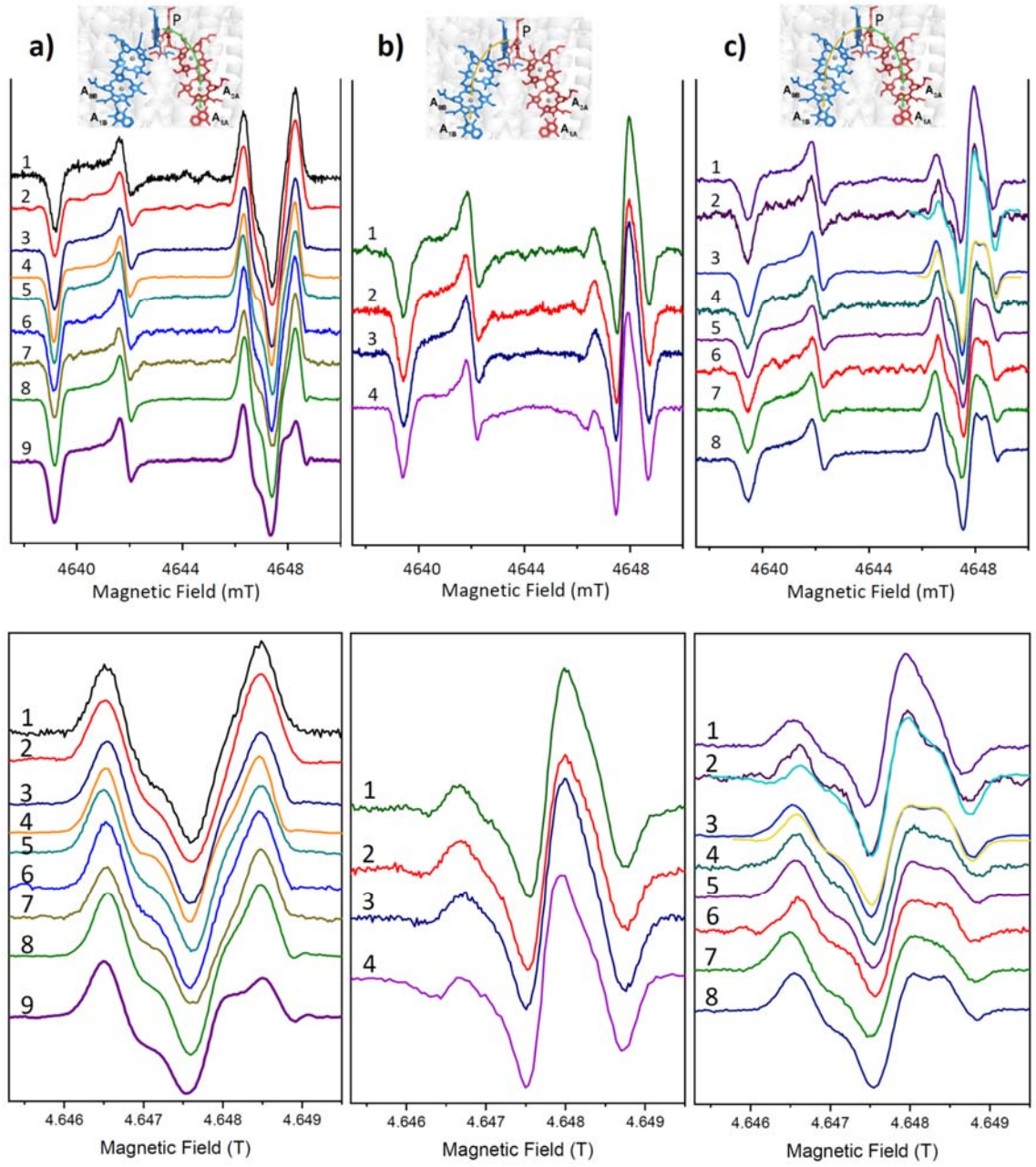

Figure S2. Experimental 130 GHz TR-EPR spectra of PSI complexes from fully deuterated cyanobacterium Synechococcus leopoliensis, recorded at different temperatures, different freezing and illumination conditions, and from different preparation batches. Red cofactors belong to the A-branch, and blue cofactors to the B-branch. **Top.** Identical to Figure 4 in the manuscript. **Bottom.** High-field part of the SCRP spectra of (**a**) $P^{+}A_{1A}^{-}$, in the "A-branch only sample", (**b**) $P^{+}A_{1B}^{-}$, in the "B-branch only sample", and (**c**) in $P^{+}A_{1A}^{-}$ and $P^{+}A_{1B}^{-}$ in "AB-branch sample" at different temperatures as detailed in Figure 4.

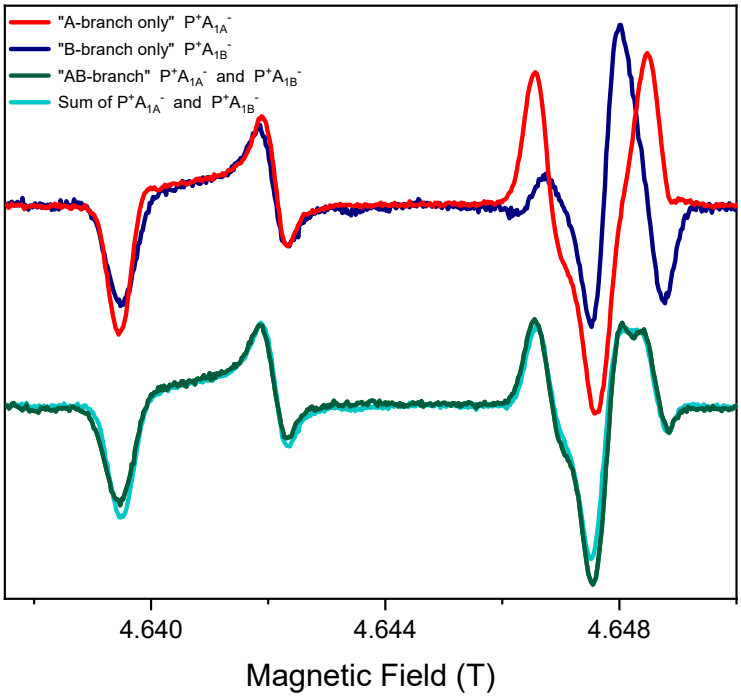

Figure S3. Comparison of experimental high frequency TR-EPR line shapes of the SCRP for $P^+A_{1A}^-$, in the "A-branch only sample" (red), $P^+A_{1B}^-$, in the "B-branch only sample" (blue), and $P^+A_{1A}^-$ and $P^+A_{1B}^-$ in "AB-branch sample" (olive). Cyan – is sum (1:1) of two experimental spectra on the top: $P^+A_{1A}^-$ and $P^+A_{1B}^-$. All spectra were normalized for intensity of A_1^- g_y component (see Figure 2 main text). All spectra were recorded at 100 K. The sum of two experimental spectra match SCRP spectra from "AB-branch sample", confirming that the ratio of ET through A- and B-branches at 100 K is close to 50:50.

References of the Supporting Information

(1) Daboll, H. F.; Crespi, H. L.; Katz, J. J. Mass Cultivation of Algae in Pure Heavy Water. *Biotechnol. Bioeng.* **1962**, *4*, 281-297.

(2) Utschig, L. M.; Chen, L. X.; Poluektov, O. G. Discovery of Native Metal Ion Sites Located on the Ferredoxin Docking Side of Photosystem I. *Biochemistry* **2008**, *47*, 3671-3676.

(3) Parret, K. G.; Mehari, T.; Warren, P. G.; Golbeck, J. H. Purification and Properties of the Intact P_{700} and F_x-Containing Photosystem I Core Protein. *Biochem. Biophys. Acta* **1989**, *973*, 324.

(4) Warren, P. V.; Parrett, K. G.; Warden, J. T.; Golbeck, J. H. Characterization of a Photosystem I Core Containing P_{700} and Intermediate Electron Acceptor A_1. *Biochemistry* **1990**, *29*, 6545-6550.

(5) Poluektov, O. G.; Utschig, L. M.; Schlesselman, S. L.; Lakshmi, K. V.; Brudvig, G. W.; Kothe, G.; Thurnauer, M. C. Electronic Structure of the P_{700} Special Pair from High-Frequency Electron Paramagnetic Resonance Spectroscopy. *J. Phys. Chem. B* **2002**, *106*, 8911-8916.

(6) Bresgunov, A. Y.; Dubinskii, A. A.; Krimov, V. N.; Petrov, Y. G.; Poluektov, O. G.; Lebedev, Y. S. Pulsed EPR in 2 mm Band. *Appl. Magn. Reson.* **1991**, *2*, 715-728.

(7) Closs, G. L.; Forbes, M. D. E.; Norris, J. R. Spin-Polarized Electron Paramagnetic Resonance Spectra of Radical Pairs in Micelles. Observation of Electron Spin Spin Interactions. *J. Phys. Chem.* **1987**, *91*, 3592-3599.

(8) Hore, P. J. In *Advanced EPR - Applications in Biology and Biochemistry*; Hoff, A. J., Ed.; Elsevier: Amsterdam, 1989; pp 405-440.

(9) Kothe, G.; Thurnauer, M. C. What you Get Out of High-Time Resolution Electron Paramagnetic Resonance: Example from Photosynthetic Bacteria. *Photosynth. Res.* **2009**, *102*, 349-365.

(10) van der Est, A. Transient EPR: Using Spin Polarization in Sequential Radical Pairs to Study Electron Transfer in Photosynthesis. *Photosynth. Res.* **2009**, *102*, 335-347.

(11) Stehlik, D.; Golbeck, J. H. In *Photosystem I: The Light-Driven Plastocyanin:Ferredoxin Oxidoreductase*; Govindjee, Ed.; Springer: Dordrecht, The Netherlands, 2006; pp 361-386.

(12) Thurnauer, M. C.; Poluektov, O. G.; Kothe, G.; Golbeck, J. H. In *Photosystem I: The Light-Driven Plastocyanin:Ferredoxin Oxidoreductase*; Govindjee, Ed.; Springer: Dordrecht, The Netherlands, 2006; pp 339-360.

(13) van der Est, A.; Golbeck, J. H. In *Photosystem I: The Light-Driven Plastocyanin:Ferredoxin Oxidoreductase*; Govindjee, Ed.; Springer: Dordrecht, The Netherlands, 2006; pp 387-411.

(14) Bittl, R.; Weber, S. Transient Radical Pairs Studied by Time-Resolved EPR. *Biochim. Biophys. Acta* **2005**, *1707*, 117-126.

(15) Buckley, C. D.; Hunter, D. A.; Hore, P. J.; McLauchlan, K. A. Electron Spin Resonance of Spin-Correlated Radical Pairs. *Chem. Phys. Lett.* **1987**, *135*, 307-312.

(16) Hore, P. J.; Hunter, D. A.; McKie, C. D.; Hoff, A. J. Electron Paramagnetic Resonance of Spin-Correlated Radical Pairs in Photosynthetic Reactions. *Chem. Phys. Lett.* **1987**, *137*, 495-500.

(17) Bittl, R.; Zech, S. G. Pulsed EPR Spectroscopy on Short-Lived Intermediates in Photosystem I. *Biochim. Biophys. Acta* **2001**, *1507*, 194-211.

(18) van der Est, A. Light-Induced Spin Polarization in Type I Photosynthetic Reaction Centres. *Biochim. Biophys. Acta* **2001**, *1507*, 212-225.

(19) Poluektov, O. G.; Paschenko, S. V.; Utschig, L. M.; Lakshmi, K. V.; Thurnauer, M. C. Bidirectional Electron Transfer in Photosystem I: Direct Evidence from High-Frequency Time-Resolved EPR Spectroscopy. *J. Am. Chem. Soc.* **2005**, *127*, 11910-11911.

(20) van der Est, A.; Prisner, T.; Bittl, R.; Fromme, P.; Lubitz, W.; Möbius, K.; Stehlik, D. Time Resolved X-, K-, and W-band EPR of the Radical Pair State $P_{700}^{\cdot+}A_1^{\cdot-}$ of Photosystem I in Comparison with $P_{865}^{\cdot+}Q_A^{\cdot-}$ in Bacterial Reaction Centers *J. Phys. Chem. B* **1997**, *101*, 1437-1443.

(21) Jordan, P.; Fromme, P.; Witt, H. T.; Klukas, O.; Saenger, W.; Krauss, N. Three-Dimensional Structure of Cyanobacterial Photosystem I at 2.5 Å Resolution. *Nature* **2001**, *411*, 909-917.

(22) Käss, H.; Fromme, P.; Witt, H. T.; Lubitz, W. Orientation and Electronic Structure of the Primary Donor Radical Cation P_{700}^{+} in Photosystem I: A Single Crystals EPR and ENDOR Study. *J. Phys. Chem. B* **2001**, *105*, 1225-1239.

(23) Webber, A. N.; Lubitz, W. P700: the Primary Electron Donor of Photosystem I. *Biochim. Biophys. Acta* **2001**, *1507*, 61-79.